Fluid-Mineral Interactions: A Tribute to H. P. Eugster
© The Geochemical Society, Special Publication No. 2, 1990
Editors: R. J. Spencer and I-Ming Chou

Crystallization history of a pyroxenite xenolith in a granulite inferred from chemical and single-crystal X-ray data

JIŘÍ FRÝDA
Geological Survey, Malostranské náměstí 19, 118 21 Praha 1, Czechoslovakia

and

MILAN RIEDER
Institute of Geological Sciences, Charles University, Albertov 6, 128 43 Praha 2, Czechoslovakia

Abstract—Porphyroclasts of orthopyroxene and clinopyroxene in the pyroxenite have bulk compositions corresponding to an equilibrium at about 1260°C and their content of Fe^{3+} indicates a relatively high oxygen fugacity during their crystallization. Later they were corroded during recrystallization by a reaction with olivine that yielded spinel grains and pyroxene neoblasts. This reaction proceeded in the subsolidus, under increasingly reducing conditions, and produced spinel of progressively smaller grain size and increasing Al content. Finally, at about 910°C, the recrystallization ceased, at approximately the same time as the porphyroclasts underwent exsolution. Orthopyroxene porphyroclasts exsolved clinopyroxene and spinel lamellae, crystallographically oriented in the host. Clinopyroxene porphyroclasts probably exsolved enstatite first and then spinel, as a result of a strong reduction probably caused by the diffusion of hydrogen. Oxygen, thus freed, combined with hydrogen, yielding about 2.5 OH per seven R^{2+} in the exsolved enstatite and converted it into an orthoamphibole-like phase that is perfectly crystallographically aligned in the host. It appears that the unmixing of spinel lamellae may be viewed as a redox reaction and that concomitantly forming hydrated phases may serve as a proof of the role of hydrogen during the evolution of mantle xenoliths.

GEOLOGICAL SETTING

THE XENOLITH of olivine websterite studied comes from the abandoned Lichtenštejn quarry located on the SSW slope of Mount Kleť, about 1.5 km from the village of Vyšný near Český Krumlov, southwestern Czechoslovakia. The xenolith is about 70 cm in diameter, embedded in a relatively homogeneous, partly recrystallized kyanite-garnet felsic granulite, which belongs to the Blanský les Mountains Massif, one of the largest granulite massifs of the Moldanubian crystalline complex. While numerous ideas on the genesis of the granulites in the area have been put forth, it is generally agreed that they formed at high pressures, near the base of the Earth's crust (VRÁNA, 1987; FIALA *et al.*, 1987). Ultramafic rocks such as dunites, lherzolites, harzburgites, and olivine websterites (most of them carrying pyrope garnet) represent about 5 vol.% of the rocks of the Blanský les Mountains Massif, and so far they have received relatively little attention. Further details about the geology of the area can be found in papers by FEDIUKOVÁ (1965, 1978), ROST (1966), KODYM (1972), KODYM *et al.* (1978), VRÁNA (1979, 1987), SLABÝ (1983), or FIALA *et al.* (1987). The papers by VAN BREEMEN *et al.* (1982) and AFTALION *et al.* (1989) deal with geochronology.

PETROGRAPHY

The studied xenolith contains orthopyroxene (OPX), clinopyroxene (CPX), olivine (OL), and spinel (SPN). The minerals vary in proportion, so the volume percentages (OPX 45–65%, CPX 15–25%, OL 15–30%, SPN < 3%) are only approximate. Nevertheless, according to Streckeisen's (1973) classification, the rock can be referred to as olivine websterite.

Orthopyroxene is present in what appears to be two generations. The first is large lamellar porphyroclasts (up to 2 cm in size, Fig. 1), the second, smaller lamellae-free neoblasts (<2 mm). The porphyroclasts are irregularly shaped because of corrosion during recrystallization, but remain elongated parallel to [001]. They are intensely bent and often kinked along deformation planes roughly perpendicular to [001], along which smaller fragments separated (Fig. 1). This deformation cannot be younger than the exsolution of lamellae; if it were, we would not observe SPN grains to follow deformation zones nor would the lamellae there be by about an order of magnitude thicker than in unaffected parts of the porphyroclasts (Fig. 2). The density of lamellae is uniform throughout the grains all the way to the border with other pyroxene grains. However, along contacts with olivine, there may be

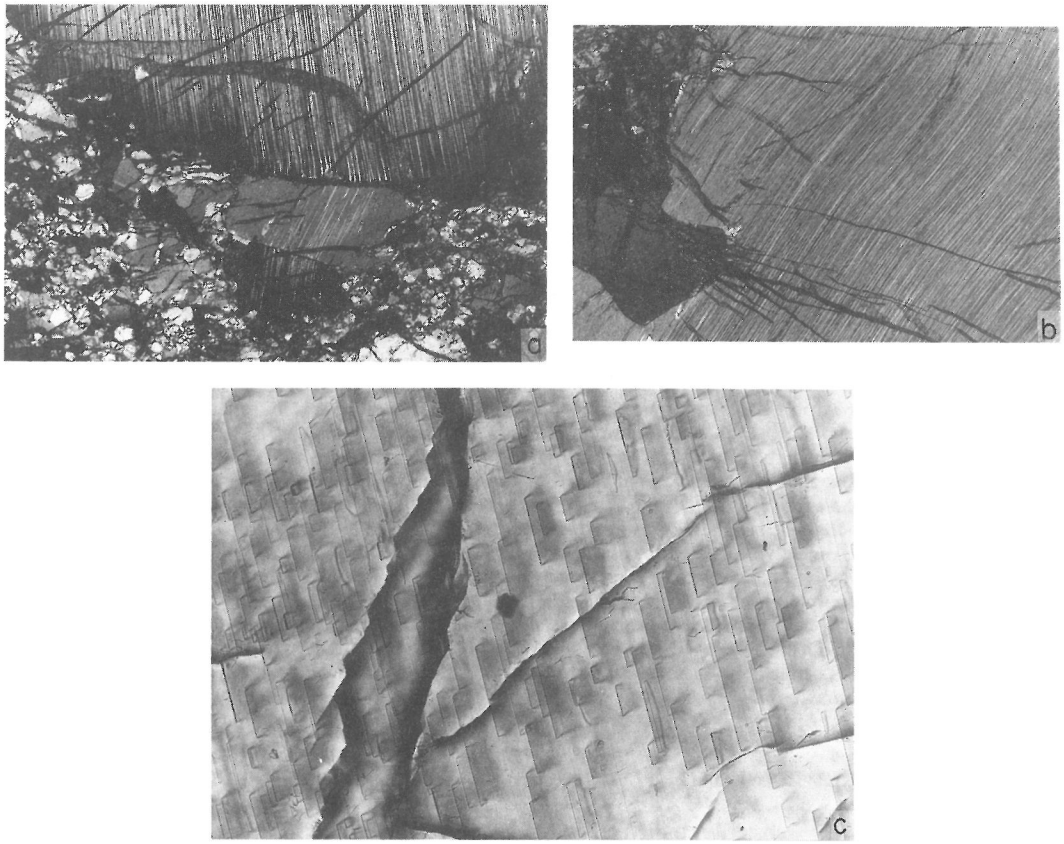

FIG. 1. a. Orthopyroxene porphyroclast, deformed and broken, surrounded by recrystallization products. Lamellae-free zones in the porphyroclast rim recrystallized olivine grains. Crossed polars, width of photograph = 4 mm. b. A plastically deformed OPX porphyroclast corroded during recrystallization. Olivine in the lower left-hand corner exhibits wavy extinction. The lamellae in OPX do not seem to disappear along $[100]_{OPX}$ as readily as along directions in the $(100)_{OPX}$ plane. Crossed polars, width of photograph = 4 mm. c. Lamellae of spinel (SPN) in OPX porphyroclast seen in a section roughly perpendicular to $[001]_{OPX}$. The SPN platelets lie parallel to $(100)_{OPX}$ and apparently contribute to the easy parting along that plane. Plane-polarized light, width of photograph = 0.5 mm.

a lamellae-free margin (0.5–1.0 mm thick). Contrary to porphyroclasts, neoblasts do not show deformation, and occur jointly with recrystallized olivine and large (vermicular) grains of spinel.

Clinopyroxene porphyroclasts reach up to 7 mm in size and contain abundant lamellae (Figs. 2 and 3) evenly distributed throughout except for lamellae-free zones, about 0.5 mm wide, that follow the border with OL grains. Clinopyroxene porphyroclasts do not show signs of plastic deformation, but many are fragmented. Small lamellae-free fragments surrounded by olivine cannot be distinguished from possible CPX neoblasts.

The mean size of OL grains is about 4 mm, larger grains are elongate and often penetrated by kink bands. The larger grains also contain zones or veils of isometric inclusions that were not studied further (Fig. 3), but appear like CO_2- or CO-containing fluid inclusions known from mantle xenoliths (Fig. 3; KIRBY and GREEN, 1980, pl. 4-D; ANDERSON *et al.*, 1984, Fig. 1-E, F; BERGMAN and DUBESSY, 1984, Fig. 2a, b). The zones of inclusions seem to have no crystallographic orientation and appear not to have a systematic relation to kink bands. The rock also contains small OL grains free from signs of deformation or inclusions which always accompany OPX neoblasts and vermicular spinel.

Spinel is red-brown, and its large (vermicular) grains or aggregates, which represent the vast majority of spinel in the rock, may reach 5 mm across. They do not seem to associate preferentially with any of the three primary minerals in the xenolith. Contacts of OPX and CPX porphyroclasts are punctuated with chains of SPN grains (Fig. 3) rang-

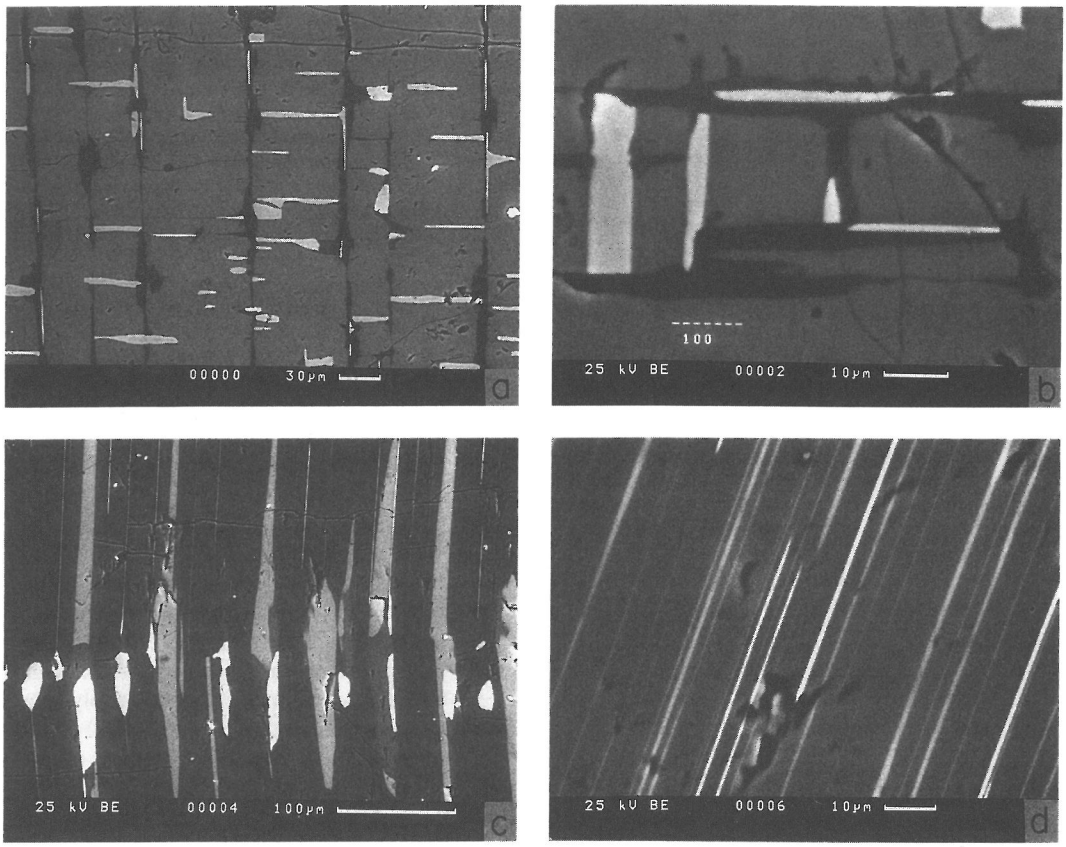

FIG. 2. Back-scattered electron images of pyroxene porphyroclasts. a, b. Section across a CPX porphyroclast, approximately perpendicular to $[001]_{CPX}$. Most spinel lamellae (white) are parallel to $(010)_{CPX}$ and lamellae of the orthoamphibole phase (OA, black) are mostly parallel to $(100)_{CPX}$, but there are some exceptions. The 'wrong' orientation of SPN lamellae seems to be associated with the OA phase. The $(100)_{CPX}$ is vertical in a. and horizontal in b. c. OPX porphyroclast, cut roughly perpendicular to $[010]_{OPX}$, showing a deformation zone with swollen CPX lamellae (light grey) and enriched in SPN grains (white). d. A section of OPX porphyroclast, approximately parallel to $[001]_{OPX}$, illustrating the distribution of lamellae of SPN (white) and CPX (light grey).

ing between 10^{-3} and 10^{-1} mm in size. Similar grains of spinel ($<10^{-2}$ mm) occur along deformation zones in OPX porphyroclasts (Fig. 2) or inside OL crystals.

In the nomenclature of MERCIER and NICOLAS (1975), the texture of the Lichtenštejn quarry xenolith is porphyroclastic. These authors cite the inclusion of spinel in olivine as evidence of a recrystallization of olivine, following an intensive deformation. However, such an effect is typical of the genetically younger equigranular texture, and thus we may refer to the present texture as transitional between porphyroclastic and equigranular.

EXPERIMENTAL

Single-crystal X-ray work was done on a Dioptra precession camera (HANIC *et al.*, 1955). Powder data were recorded on a DRON-2,0 diffractometer (Burevestnik, Leningrad), with scanning speed 0.5° (2θ)/minute, and processed by BURNHAM's (1962) least squares program. The cell edge of spinel was based on film data extrapolated against the Nelson-Riley function (RIEDER, 1971).

An ARL-SEMQ microprobe was used to obtain chemical compositions. The accelerating voltage was 15 kV, current 50 nA, and counting time 20 seconds. Natural silicate minerals were used as standards for Ti, Cr, Mn, Si, Fe, K, Na, Mg, Ca, and Al, and synthetic Ni olivine was used for Ni. Analytical points were selected after observation in back-scattered electron mode (accelerating voltage 30–35 kV). Five to ten grains of each type of mineral (porphyroclast, neoblast, lamella) were analyzed. If homogeneous, the mineral was analyzed at three to six points, otherwise, up to 25 analyses were made. The Ca in olivine and Ni in OL, OPX, CPX, SP were determined with 100 nA current and 100 seconds counting time (used for Ca by ADAMS and BISHOP, 1986). The bulk composition of OPX and CPX porphyroclasts was analyzed either using a defocussed electron beam (35 μm) or by allowing

the beam to scan over rasters, 50 × 50 μm, that were combined so as to pave stretches several hundred μm in diameter. Both methods yielded practically identical results. After corrections for drift of the instrument and for dead time of the detectors, the data were reduced according to BENCE and ALBEE (1968). When assessing the bulk chemical compositions, one must be aware that the uncertainties may exceed the errors indicated because the assumption of a homogeneous distribution of each element in the X-ray generation range is not fulfilled. Standard errors of individual determinations were computed according to KOTRBA (1989).

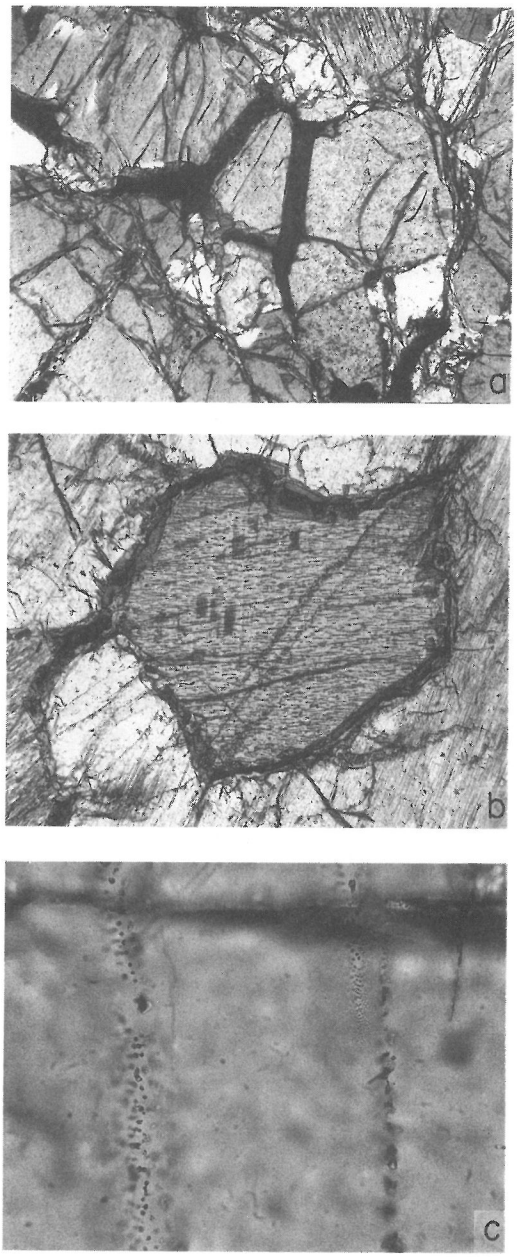

FIG. 3. a. Spinel (black) surrounds OPX neoblasts (light grey) or is enclosed in olivine neoblasts (white, lower right-hand corner). Crossed polars, width of photograph = 2 mm. b. A CPX porphyroclast with abundant lamellae, surrounded by OPX porphyroclasts. Chains of spinel grains (black) follow grain boundaries. Crossed polars, width of photograph = 2 mm. c. Veils of inclusions in a crystal of deformed olivine. Plane-polarized light, width of photograph = 0.2 mm.

PHASE BOUNDARIES AND LATTICE ROTATION

Assuming coherency between lamellae and host, the orientation of phase boundaries and the corresponding lattice rotation can be calculated (ROBINSON *et al.*, 1977; FLEET, 1981, 1982; ŠANC and RIEDER, 1983). Two models were used here and applied to the following intergrowths: CPX lamellae & OPX host, SPN lamellae & CPX host, and SPN lamellae & OPX host. No calculation involving the orthoamphibole phase (OA, see below) was performed because it appears to have formed by secondary replacement and not by a process amenable to the above numerical treatment. Relatively good precision powder cell data were used for CPX and OPX, but for SPN we had to use the less precise single-crystal cell edge because it is the only one we had for spinel in lamellae. These unit-cell data were extrapolated to high temperatures using the thermal expansion data of SKINNER (1966) and ŠANC (1982). Correction for the effect of pressure and for chemical changes after coherency had been lost were not made. The unit-cell data were then converted to equivalent subcells common to both phases in an intergrowth pair, based on near-coincidence of reflections in precession photographs, and these, in turn, were input into the calculations. The results are summarized in Table 1. Perhaps the most interesting among them is the lattice rotation of SPN in OPX host whose measured value (0.81(3)°) corresponds well to the measured 0.86(3)° reported for the same pair from Tři Studně (ŠANC and RIEDER, 1983).

ORTHOPYROXENE PORPHYROCLASTS

All six crystals examined by X-ray precession contain CPX and SPN lamellae (Fig. 2); their unit-cell data appear in Table 2. Each of the two exsolved phases is present in two orientations. The relations in this standard intergrowth are illustrated in Fig. 7 of ŠANC and RIEDER (1983). The dominant faces of all lamellae are parallel to (100) of host OPX. Clinopyroxene lamellae are less than 4 μm thick,

Table 1. Measured and calculated phase boundaries

Host Phase	OPX	OPX	CPX
Lamella	CPX	SPN	SPN
Coherent Composition Plane Parallel to	$[010]_{CPX} \parallel [010]_{OPX}$	$[100]_{OPX} \parallel [111]_{SPN}$	$[010]_{CPX} \parallel [\bar{1}10]_{SPN}$
Lattice Rotation	$[100]^*_{CPX} \wedge [100]^*_{OPX}$	$[010]^*_{OPX} \wedge [\bar{1}10]^*_{SPN}$	$[100]^*_{CPX} \wedge [111]^*_{SPN}$
Measurements[a]			
Lattice Rotation	0.0(3)°	0.81(3)°	0.0(3)°
Composition Plane I $\wedge$ $[001]_{host}$	0.(5.)°	40.(20.)°	[d]
Composition Plane II $\wedge$ $[001]_{host}$	0.(5.)°	−40.(20.)°	[d]
Calculations[a,b]			
Area Robinson[c]			
Lattice Rotation I	−0.19° to −0.22°	0.52° to 0.54°	1.55° to 2.54°
Composition Plane I $\wedge$ $[001]_{host}$	−2.95° to −6.54°	32.8° to 49.6°	49.9° to 60.3°
Lattice Rotation II		−0.52° to −0.54°	2.12° to 3.93°
Composition Plane II $\wedge$ $[001]_{host}$		−32.8° to −49.6°	56.6° to 73.1°
Vector Robinson[c]			
Lattice Rotation I	−0.11° to −0.20°	0.0°	−0.15° to −0.19°
Composition Plane I $\wedge$ $[001]_{host}$	−4.10° to −10.80°	0.0°	26.7° to 27.7°
Lattice Rotation II			−5.48° to −5.66°
Composition Plane II $\wedge$ $[001]_{host}$			83.4° to 83.9°

[a] When viewed along $[010]_{host}$, angles measured in counter-clockwise direction are given as positive.
[b] Calculations are presented as intervals corresponding to 20° and 1000°C, respectively.
[c] 'Vector Robinson' is the approach of ROBINSON *et al.* (1977), 'area Robinson' is a modification of ŠANC and RIEDER (1983).
[d] Could not be measured.

their length along $[010]_{OPX}$ and $[001]_{OPX}$ reaches several tenths of a mm; and they are 10–30 μm apart. Spinel lamellae are thinner (≤ 2 μm) and distinctly longer along $[001]_{OPX}$ (up to 1 mm) than along $[010]_{OPX}$. Their termination appears to be tilted relative to $[010]_{OPX}$, towards $[010]_{OPX}$ in some lamellae, and $[0\bar{1}0]_{OPX}$ in others, under angles about 40°. The uncertainty of this angle is large, perhaps up to 20°. The observed orientations and morphologies are those predicted from the theory of optimal phase boundaries (Table 1).

The $Mg/(Mg + Fe_{tot})$ and $Ca/(Ca + Mg + Fe_{tot} + Mn)$ ratios of OPX host are, respectively, 0.911(2) and 0.005(1) (Fig. 4). The differences between the composition of OPX host from cores and from margins of the porphyroclasts were less than the error of analysis. However, the ranges obtained for Al_2O_3 and Cr_2O_3 are wider, namely 2.95–3.85 wt.% and 0.29–0.55 wt.%, respectively, and the Cr/Al ratio varies from 0.062 to 0.102 (Fig. 5). These elements indeed are those that can be expected to vary if a lamella of SPN or CPX is accidentally present in the X-ray generation range of an analytical point in OPX host.

Table 2. Unit-cell data for phases in pyroxene porphyroclasts and spinel

	OPX porphyroclasts				CPX porphyroclasts				
	OPX host		CPX lamellae	SPN lamellae	CPX host		OA lamellae	SPN lamellae	Spinel large grains
a, nm	1.822(1)	1.829(1)	0.975(2)	0.8138(8)	0.9735(5)	0.975(1)	1.83(1)	0.815(1)	0.8156(1)
b, nm	0.8813(9)	0.882(1)	0.895(2)		0.8910(5)	0.8915(8)	1.81(1)		
c, nm	0.5195(3)	0.5188(5)	0.5252(9)		0.5251(3)	0.5258(6)	0.524(2)		
β, °	90.0	90.0	105.78(17)		105.93(2)	106.05(15)	90.0		
Method	[a]	[b]	[b]	[b]	[a]	[b]	[b]	[b]	[c]

[a] Powder data, DRON-2,0 diffractometer, graphite-monochromatized Cu radiation, least-squares refinement by program of Burnham (1962).
[b] Measurements of precession photographs; the data given are means weighted in proportion to the number of reciprocal rows measured in individual photographs.
[c] Cylindrical camera, $2r = 114.59$ mm, extrapolation against the function of Nelson and Riley.

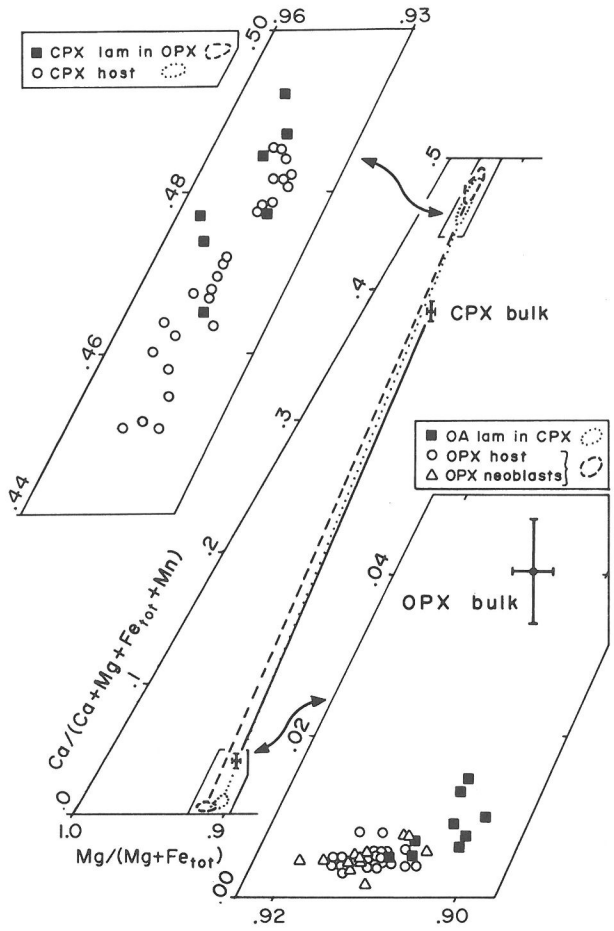

FIG. 4. Relations between phases in pyroxene porphyroclasts. The error crosses for the bulk compositions embrace $\pm 1\sigma$. The full tieline is that for primary equilibrium of bulk porphyroclasts, the dotted tieline is for compositions of breakdown phases in CPX porphyroclasts, the dashed tieline is for the same in OPX porphyroclasts. The points for bulk composition of the porphyroclasts fall off tielines for the breakdown phases because the bulks include spinel richer in iron.

Clinopyroxene lamellae could be analyzed only in deformation zones where their thickness increases (Fig. 2). The mean values of the $Mg/(Mg + Fe_{tot})$ and $Ca/(Ca + Mg + Fe_{tot} + Mn)$ ratios are 0.948(5) and 0.481(9), respectively (Fig. 4). The ratio Cr/Al equals 0.102–0.162 (Fig. 5).

Spinel lamellae too could be analyzed only when swollen. Their $Mg/(Mg + Fe_{tot})$ ratio falls between 0.754 and 0.777, the $Cr/(Cr + Al)$ ratio ranges from 0.144 to 0.161 (Fig. 6). The content of Fe^{3+} was calculated assuming full cation occupancy and charge neutrality (Fig. 7). Spinel grains following deformation zones in the porphyroclasts have a higher $Mg/(Mg + Fe_{tot})$ ratio (0.779–0.783), and the same applies to the $Cr/(Cr + Al)$ ratio (0.158–0.169). The contents of Mn and Fe^{3+} are identical with those of SPN lamellae.

The bulk composition of OPX porphyroclasts is well characterized by their mean values (Table 3, Fig. 4) inasmuch as individual analyses differ by less than the error of analysis. The ratio $Mg/(Mg + Fe_{tot}) = 0.908(2)$ is lower than that of the OPX host; this is due to the very low $Mg/(Mg + Fe_{tot})$ of the SPN lamellae. Mean $Ca/(Ca + Mg + Fe_{tot} + Mn) = 0.040(7)$ and $Cr/Al = 0.13(3)$. The bulk composition of cores of porphyroclasts is constant within the error of analysis, but towards contacts with olivine, the contents of Ca, Cr, and Al smoothly decrease, which is manifest as thinning and disappearance of CPX and SPN lamellae.

CLINOPYROXENE PORPHYROCLASTS

Five crystals were X-rayed to determine the mutual orientations of phases, that is the CPX host

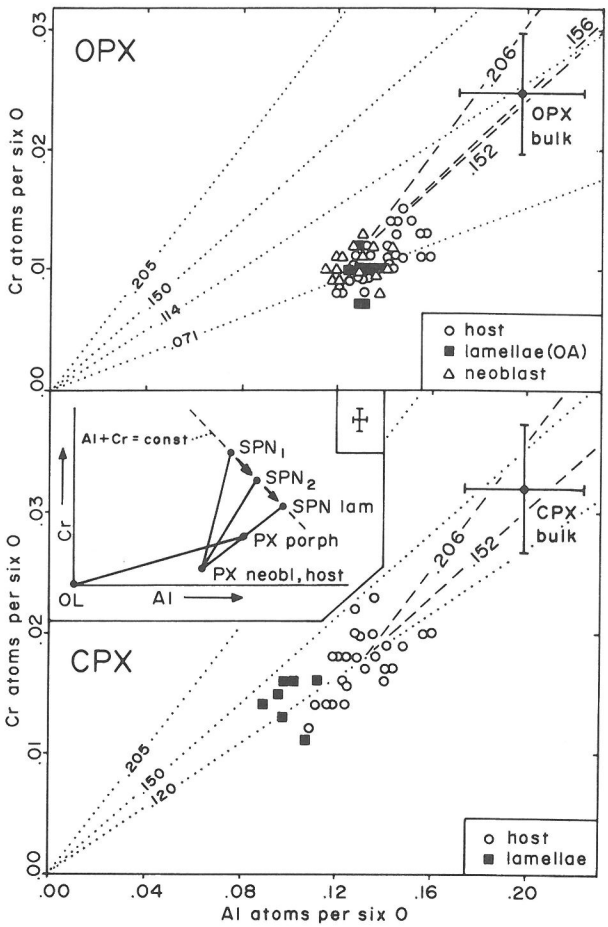

FIG. 5. The relation between Cr and Al in breakdown pyroxenes and orthoamphibole (OA); a cross of error bars 3σ in length is shown in a rectangle. The composition of bulk porphyroclasts is known with a much lower precision, the crosses indicate $\pm 1\sigma$. Dotted lines are labeled with Cr/(Cr + Al) ratios. Dashed lines emanate from points representing means for the clusters of data and are labeled with Cr/(Cr + Al) ratios of associated spinels. In the inset appears a schematic illustration of the reaction of pyroxene porphyroclasts with olivine to PX neoblasts and an older spinel (SPN_1), then to a younger spinel (SPN_2) and ending with unmixed SPN lamellae formed without the participation of olivine.

and lamellae of spinel and an orthorhombic amphibole-like phase, possibly related to anthophyllite (OA, Fig. 2). Spinel is present in two orientations whose volumes were nearly identical in OPX porphyroclasts, but clearly differ here: there is always more spinel in B orientation than in A (labeling of ŠANC and RIEDER, 1983). The intensities of reflections of SPN_A correlate positively with those of OA indicating that lamellae of SPN_A associate with OA lamellae. Exactly the same was observed in CPX porphyroclasts from Tři Studně (ŠANC and RIEDER, 1983; Fig. 6) except that the phase in lamellae was orthopyroxene rather than orthoamphibole.

Characterization of the orthoamphibole phase is admittedly incomplete. First, the intensities of its reflections are much weaker than those of the host because of the relative volumes involved and, second, there is the unavoidable overlapping of reflections (Fig. 8). Nonetheless it was identified in all crystals examined. The reciprocal cell geometry and the intensity distribution agree with the Laue group *mmm*, but a complete diffraction symbol could not be assigned. There is a good agreement of the unit-cell data and a reasonably good overall agreement of intensities calculated for anthophyllite with the ones observed in the X-ray photographs, but there are some disturbing dissimilarities. For instance, the reflections 052, 072, 043, and 083, which are not

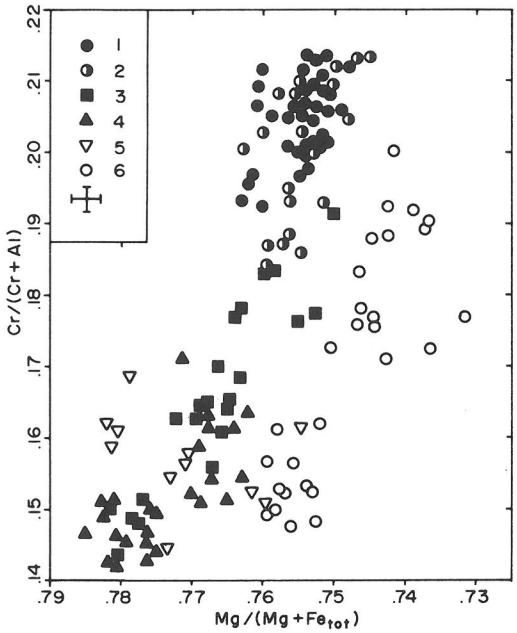

FIG. 6. The relation between chemistry and paragenetic position of spinel. The cross of error bars 3σ in length is shown in the symbol rectangle. 1 = large grains not associated with pyroxene neoblasts; 2 = rims of large grains; 3 = medium and small grains; 4 = lamellae in clinopyroxene; 5 = lamellae and grains in orthopyroxene; 6 = grains enclosed in aggregates of olivine.

permitted in space group *Pnma* (that of anthophyllite) are well visible in the photographs (Fig. 8), while several $4k0$ reflections and the strong 161, which should be present in patterns of anthophyllite, were not observed. Therefore, the identification remains tentative at best. Perhaps more could be learned by a high-resolution electron microscopic examination, but no such study has been contemplated yet.

The OA phase is well visible in back-scattered electron images, but it is all but invisible with petrographic microscopy. It forms lamellae with a variable thickness and irregular outline (Fig. 2); most of them are parallel to $(100)_{CPX}$. The lamellae are distributed evenly throughout the host, with a spacing of 30–80 μm. Some OA lamellae are parallel to $(010)_{CPX}$, and the largest pods of OA occur at intersections of both lamellar systems. It can be seen that there are two systems of lamellae of spinel, one associated with the CPX host, the other, with OA lamellae. The first lamellae are parallel to $(010)_{CPX}$, and their thickness is mostly between four and ten μm. The second SPN lamellae are usually thinner and often outgrow the OA phase and continue, with unchanged morphology, into CPX (Fig. 2). It is important that most SPN lamellae parallel to $(010)_{CPX}$ terminate at OA or at SPN lamellae that are parallel to $(100)_{CPX}$. This indicates that the unmixing of the OA phase (or rather its precursor's) began before the formation of SPN lamellae parallel to $(010)_{CPX}$. In sections parallel to $(010)_{CPX}$, one can see that the spinel lamellae belong in fact to two morphologies like those observed at Tři Studně (ŠANC and RIEDER, 1983, Fig. 11). The SPN lamellae associated with the OA phase belong to one morphological type, being elongated on $[001]_{CPX}$. The den-

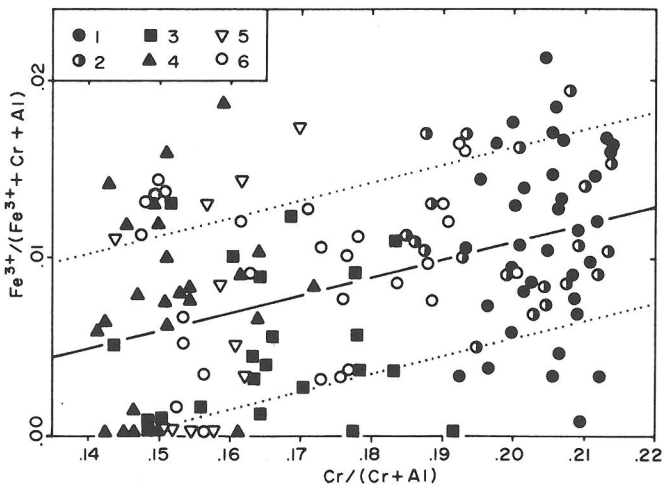

FIG. 7. Calculated trivalent iron increases in spinels richer in Cr. A few analyses whose Fe^{3+} calculated as negative were plotted at $Fe^{3+} = 0$. Correlation coefficient for the regression $r = 0.392$, dotted lines indicate $\pm 1\sigma$. Symbols as in Fig. 6.

Table 3. Chemical composition of orthopyroxene and the orthoamphibole-like phase (OA)

	OPX porphyroclast bulk mean[a]	OPX host		OA lamellae		OPX neoblast	
		Typical analysis[b]	Range	Typical analysis[b]	Range	Typical analysis[b]	Range
SiO_2	53.5(7)	55.1(4)	53.9–56.2	55.0(4)	54.7–55.5	55.5(4)	55.1–56.2
TiO_2	0.04(3)	0.04(2)	0.00–0.10	0.02(2)	0.00–0.04	0.04(2)	0.00–0.09
Al_2O_3	4.8(7)	3.40(4)	2.95–3.85	3.20(4)	3.10–3.40	3.15(4)	2.84–3.50
Cr_2O_3	0.9(2)	0.40(2)	0.29–0.55	0.37(2)	0.28–0.45	0.40(2)	0.29–0.47
FeO	5.9(1)	6.01(5)	5.65–6.24	6.38(5)	6.00–6.61	5.96(5)	5.90–6.18
MnO	0.14(2)	0.14(2)	0.06–0.18	0.14(2)	0.11–0.20	0.14(2)	0.06–0.19
MgO	32.6(5)	34.8(2)	33.5–35.7	34.1(2)	33.8–35.0	34.6(2)	34.0–35.3
CaO	2.1(4)	0.27(2)	0.19–0.41	0.46(2)	0.29–0.75	0.27(2)	0.10–0.42
NiO	[c]	0.095(5)	0.09–0.10	[c]	[c]	[c]	[c]
Na_2O	0.04(1)	0.02(1)	0.00–0.04	0.0(0)	0.0	0.0(0)	0.0
K_2O	0.0(0)	0.0(0)	0.0	0.0(0)	0.0	0.0(0)	0.0
Σ	100.(1.)	100.3(5)		99.7(5)		100.1(5)	
$Mg/(Mg + Fe_{tot})$	0.908(2)	0.9116(8)	0.907–0.916	0.9050(7)	0.901–0.910	0.9119(8)	0.906–0.919
$Ca/(Ca + Mg + Fe_{tot} + Mn)$	0.040(7)	0.0051(4)	0.0036–0.0081	0.0086(4)	0.0051–0.0147	0.0051(4)	0.0015–0.0077
Cr/Al	0.13(3)	0.079(4)	0.062–0.102	0.077(4)	0.054–0.092	0.085(4)	0.063–0.100

[a] Mean of several analyses; errors reflect variation in the set on which the mean is based.
[b] Errors given are those of individual determinations and were computed according to KOTRBA (1989).
[c] Not analyzed.

sity of both the SPN and OA lamellae throughout the porphyroclasts is uniform, but it decreases in border zones adjacent to olivine grains.

The OA lamellae exhibit a constant $Mg/(Mg + Fe_{tot})$ ratio (mean 0.905(3)), and a less constant $Ca/(Ca + Mg + Fe_{tot} + Mn)$ ratio (mean 0.009(3)), Al_2O_3 and Cr_2O_3 vary between 3.10 and 3.40 wt.% and between 0.28 and 0.45 wt.%, respectively, the mean Cr/Al ratio is 0.08(2). It should be noted that the analysis of the OA phase closely resembles that of an orthopyroxene (Fig. 4), and even the total does not indicate the presence of an undetermined water content. This is analogous to what had been observed for an Mg layer silicate in similar lamellae in CPX host from Deštná (ŠANC and RIEDER, 1983), which did have a deficient analytical total.

The composition of the CPX host does not exhibit differences in the $Mg/(Mg + Fe_{tot})$ ratio between core and margin, the mean value is 0.945(3) (Figs. 4 and 9). However, the $Ca/(Ca + Mg + Fe_{tot} + Mn)$ ratio shows considerable scatter, but there appear to be no systematic differences between core and margins. There is considerable scatter in the Cr/Al ratio, with mean 0.14(2), which may be attributable to contaminations.

Also analyzed was spinel in both systems of lamellae in OPX porphyroclasts, but lamellae of the second system (associated with the OA phase) could be analyzed at a few points only, because of insufficient thickness. No differences between the two SPN lamellar systems were found. The $Mg/(Mg + Fe_{tot})$ ratio ranges from 0.762 to 0.785, $Cr/(Cr + Al)$, from 0.142 to 0.172; both correlate with each other (Fig. 6). The ratio $Fe^{3+}/(Fe^{3+} + Al + Cr)$ is below 0.02, based of course on calculated Fe^{3+}.

The bulk composition of CPX porphyroclasts (Table 4, Fig. 4) exhibits a mean $Mg/(Mg + Fe_{tot}) = 0.926(5)$, which is below that of the CPX host, due to the low $Mg/(Mg + Fe_{tot})$ ratio of SPN lamellae. The mean ratios $Ca/(Ca + Mg + Fe_{tot} + Mn)$ and Cr/Al equal 0.38(1) and 0.16(3), respectively. The bulk composition of the cores is homogeneous within analytical error.

ORTHOPYROXENE NEOBLASTS

The mean ratios $Mg/(Mg + Fe_{tot})$ and $Ca/(Ca + Mg + Fe_{tot} + Mn)$ are, respectively, 0.912(3) and 0.005(2) and are practically identical with those of the host phase in OPX porphyroclasts (Fig. 9), while the mean contents of Al_2O_3 and Cr_2O_3 are generally slightly lower (Fig. 5).

SPINEL GRAINS

Spinel grains of different morphology differ also chemically (Figs. 6, 7 and 10). Large grains of vermicular SPN (several mm across) represent over 90 vol.% of all spinel in the xenolith. They show a rather narrow variability of the $Mg/(Mg + Fe_{tot})$ and $Cr/(Cr + Al)$ ratios with means 0.754(4) and 0.206(5), respectively. Individual grains appear homogeneous, and in only a few cases, asymmetric

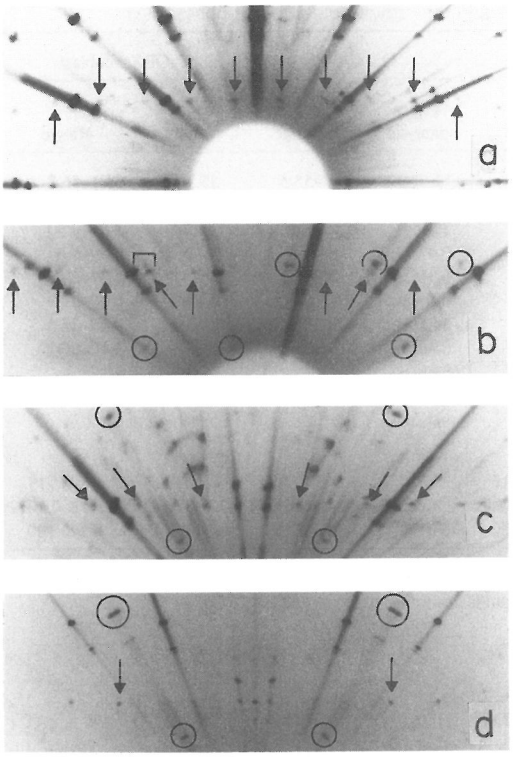

FIG. 8. Enlarged sections of precession photographs (unfiltered MoK radiation) of intergrowths involving clinopyroxene (CPX), orthoamphibole (OA), spinel (SPN), and orthopyroxene (OPX). a. Reciprocal 0*kl* net of CPX with 0*k*0, 0*k*1, and 0*k*2 rows well visible. The *hkh* net of the OA phase is superposed. Reflections in the $1k1_{OA}$ row are marked by arrows; the 171 reflection is obscured by a slightly deviating pyroxene orientation. b. Reciprocal *h*0*l* nets of CPX and OA; the *h*02 reciprocal rows of both phases coincide, reflections of OA are indicated by arrows. Also present is spinel in orientation B (*hkk* net, circles) and orientation A (small volume only) betrayed by the weak reflection within the rectangle. Reflection intensities of the $h0l_{OA}$ should obey a vertical plane of symmetry, but do not, apparently due to absorption associated with an uneven distribution of OA lamellae in the host phase. However, the symmetry plane was visible in the $h0l_{OA}$ nets of the other crystals examined. c. Reciprocal net $\bar{h}k2h$ of clinopyroxene, overlapping with the 0*kl* net of orthoamphibole and $h \cdot k \cdot -(h+k)$ net of spinel. Reflections in the 0*k*2 row of OA are marked with arrows, SPN reflections appear in circles. The strongest CPX reflections are $\bar{1}32$ and $\bar{1}32$. d. Reciprocal net 0*kl* of OPX, specifically the 0*k*2 and 0*k*3 rows, with $\bar{h}k2h$ net of CPX superposed (reflections $\bar{1}32_{CPX}$ and $\bar{1}32_{CPX}$ are shown by arrows). Note the splitting of $h \cdot k \cdot -(h+k)$ reflections of spinel (circles) caused by lattice rotation that does not operate for SPN in CPX (preceeding photograph).

zoning was encountered. The outer zones have lower Cr/(Cr + Al) and higher Mg/(Mg + Fe_{tot}) ratios, but it is likely that they in fact are an accretion of a finer grained younger spinel. The large grains have the highest ratio $Fe^{3+}/(Fe^{3+} + Al + Cr)$ of all spinel, namely 0.011(5) (Table 5).

Smaller SPN grains from contacts of pyroxene porphyroclasts exhibit more compositional variability, although individual grains are homogeneous within the error of analysis. Their Fe^{3+} calculates as lower than in large grains and the Mg/(Mg + Fe_{tot}) and Cr/(Cr + Al) ratios correlate well with each other (Figs. 6, 7). These spinels fit well into the relations between chemistry and grain size (Fig. 10).

Grains of spinel enclosed in olivine also display considerable chemical variability (Fig. 10), and their chemistry too varies with grain size. Moreover, individual grains are zoned, with Mg/(Mg + Fe_{tot}) decreasing towards contacts with olivine grains, while Cr, Al, Fe^{3+}, and Mn remain constant.

OLIVINE

Olivine occurs as large deformed grains and as smaller undeformed grains, with respective mean

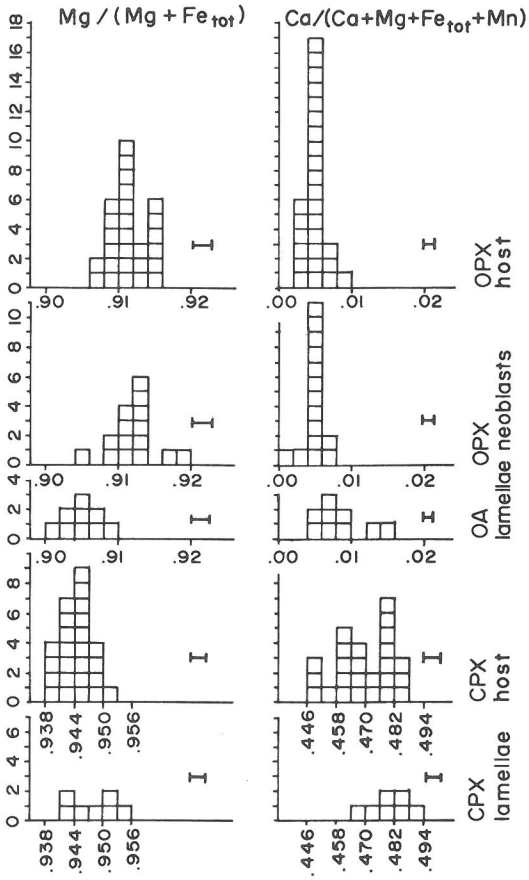

FIG. 9. Distribution of the two main compositional ratios in pyroxenes and the orthoamphibole phase (OA); one square represents one determination, the length of the error bars is 3σ.

Table 4. Chemical composition of clinopyroxene

	Porphyroclasts mean[a]	Host typical analysis[b]	Range[c]	Lamellae typical analysis[b]	Range
SiO_2	52.(1.)	53.0(4)	51.6–53.8	53.5(4)	53.0–54.4
TiO_2	0.11(4)	0.15(2)	0.10–0.21	0.11(2)	0.10–0.14
Al_2O_3	4.6(6)	3.09(4)	2.60–3.74	2.35(3)	2.12–2.65
Cr_2O_3	1.1(2)	0.63(2)	0.42–0.79	0.49(2)	0.39–0.56
FeO	2.9(2)	1.78(3)	1.64–2.04	1.68(3)	1.56–1.85
MnO	0.10(2)	0.10(2)	0.07–0.14	0.07(2)	0.04–0.12
MgO	20.2(7)	17.7(1)	17.3–18.5	17.2(1)	16.6–17.8
CaO	19.(1.)	23.1(1)	22.3–24.0	23.6(1)	22.7–24.6
NiO	[d]	0.044(5)	0.038–0.050	[d]	[d]
Na_2O	0.28(3)	0.43(2)	0.32–0.45	0.23(2)	0.19–0.27
K_2O	0.0(0)	0.0(0)	0.0	0.0(0)	0.0
Σ	100.(2.)	100.1(4)		99.2(4)	
$Mg/(Mg + Fe_{tot})$	0.926(5)	0.9466(9)	0.938–0.952	0.9480(9)	0.942–0.956
$Ca/(Ca + Mg + Fe_{tot} + Mn)$	0.38(1)	0.470(2)	0.451–0.485	0.483(2)	0.465–0.492
Cr/Al	0.16(3)	0.136(5)	0.109–0.171	0.139(6)	0.102–0.162

[a] Mean of several analyses; errors reflect variation in the set on which the mean is based.
[b] Errors given are those of individual determinations and were computed according to KOTRBA (1989).
[c] The range includes also analyses of lamellae-free fragments of porphyroclasts.
[d] Not analyzed.

values of $Mg/(Mg + Fe_{tot})$ equal to 0.907(1) and 0.9102(5). CaO is slightly higher in deformed grains, while the mean MnO and NiO contents of both types are identical (Table 6, Fig. 11). Individual olivine grains are chemically homogeneous, the only exception being zones in large deformed grains, about 0.15 mm thick, adjacent to spinel. In these zones, the $Mg/(Mg + Fe_{tot})$ increases outwards, but MnO and CaO remain constant (we did not examine the behavior of NiO).

PETROGENESIS

Textural and chemical features of the rock make it clear that at least two distinctly different processes took place.

The first process of which there is evidence involved an Al-rich orthopyroxene, an Al-rich clinopyroxene, and olivine. Despite some difficulties in obtaining the present bulk compositions of porphyroclasts and the possibility of chemical changes during recrystallization processes, there is a reasonable certainty about the temperature of primary equilibrium: the calculated temperatures based on OPX and CPX porphyroclasts fall between 1220 and 1280°C (Table 7). Such an equilibrium was not necessarily magmatic, but may have been the result of an older metamorphic-recrystallization process.

The oldest spinel (large homogeneous grains) probably did not participate in the above phase assemblage. It may have formed later by either of two processes. First, it may have been one of the products of incongruent melting of aluminous pyroxenes during partial melting, together with olivine and melt (DICKEY *et al.*, 1971; DICK, 1977a,b; MYSEN and KUSHIRO, 1977; JAQUES and GREEN, 1980). Second, it could have formed by a subsolidus metamorphic recrystallization with Al-rich pyroxene and olivine as reactants and spinel and Al-poor pyroxene as products (GREEN, 1964; OBATA, 1980; KUO and ESSENE, 1986). A variant of the second path is an unmixing process from Al-rich pyroxenes (BASU and MACGREGOR, 1975; MERCIER and NICOLAS, 1975). Spinel formed in the subsolidus would have to be in close spatial association with pyroxene neoblasts, but we observe the latter to associate with finer grained younger spinels and not with large grains (Fig. 3). This lends indirect support to the first alternative. Also the remarkable homogeneity of large SPN grains and their low $Cr/(Cr + Al)$ ratio suggest that these spinel grains formed during a weak partial melting (DICK and BULLEN, 1984; OZAWA, 1988). Inasmuch as there was a later re-equilibration between olivine and spinel, we can hardly assign meaningful temperatures to the event.

The second process which affected the rock extensively was an intensive deformation and a subsequent recrystallization. It took place at a time when the aluminous porphyroclasts became unstable and underwent the reaction,

Al-PX porphyroclast + olivine →

PX neoblast + spinel

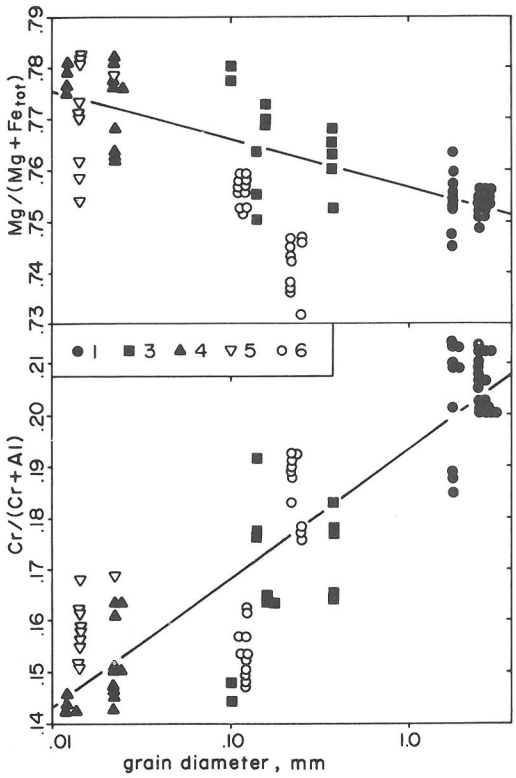

FIG. 10. The relation of the composition of spinel to grain diameter. Grain diameter is plotted logarithmically and was calculated as $(d_{min} \cdot d_{max})^{1/2}$. Inasmuch as there apparently was a cation-exchange reaction between spinel and olivine that involved Mg and Fe, points for spinel enclosed by olivine (symbol 6) were not included when the best-fit line was calculated for the top plot. No reaction with olivine involved Cr and Al, so the best-fit line in the bottom plot is based on all data points. Symbols as in Fig. 6.

(see KUO and ESSENE, 1986). The product spinel is spatially closely associated with pyroxene neoblasts (Fig. 3). The newly formed spinel exhibits mutually correlated variation of Mg/(Mg + Fe_{tot}) and Cr/(Cr + Al) (Fig. 6), which correlates also with grain size. The chemical development in time of spinel in the Lichtenštejn quarry xenolith can be referred to as an Al trend, because the smaller (and thus younger) grains exhibit progressively lower Cr/(Cr + Al) ratios. Inasmuch as one commonly finds large SPN grains with Cr/(Cr + Al) = 0.21 side-by-side with SPN lamellae whose Cr/(Cr + Al) = 0.15, the correlation of composition with grain size of spinel cannot be the result of an exchange of Al and Cr between SPN and PX similar to what had been postulated by OZAWA (1983) for Mg and Fe between SPN and OL. Also eliminated appears to be the possibility that Cr/(Cr + Al) decreased by a reaction of spinel with a trapped basaltic melt (IRVINE, 1967) or with an aluminum-rich silicate (HENDERSON, 1975). An interesting point is that the chemical composition of the smallest spinel grains is identical with that of SPN lamellae in pyroxene porphyroclasts (Fig. 6).

The set of spinel analyses from the xenolith under study falls into the fields of spinel composition from alpine-type peridotites and abyssal peridotites (DICK and BULLEN, 1984). The negative correlation between the Cr/(Cr + Al) and Mg/(Mg + Fe^{2+}) ratios in SPN from these rocks has been interpreted as a consequence of partial melting under mantle conditions (GREEN and RINGWOOD, 1967; DICK, 1977a,b,; DICK and BULLEN, 1984; OZAWA, 1988). The Cr/(Cr + Al) of spinel is thought to be an indicator of depletion of the mantle material (DICK and BULLEN, 1984). Contrary to this, at subsolidus temperatures, the distribution of Al and Cr between pyroxene and spinel appears to be independent of temperature (EALES and MARSH, 1983; OZAWA, 1988). Also the dependence of the Cr/(Cr + Al) ratio in spinel on pressure is uncertain. BASU and MACGREGOR (1975) studied spinels from ultramafic xenoliths and concluded that the Cr/(Cr + Al + Fe^{3+}) ratio increases with the depth (and thus pressure) of origin of the xenoliths, but they admit that the ratio may be a function of the bulk composition of the rocks. Experimental data of DICKEY and YODER (1972) indicate that the Cr/Al ratio of the rock dictates the distribution of Cr and Al between subsolidus SPN and CPX, and that the latter does not change with temperature or pressure.

If we accept the idea that spinel formed, together with Al-poor pyroxene, from an Al-rich pyroxene plus olivine, we must accept its consequences. Pyroxenes have two cations per three oxygens, but there are three cations per four oxygens in both olivine and spinel. Hence the quantity of product spinel must equal the quantity of reactant olivine (Fig. 5). If, however, the reaction proceeds under reducing conditions, the equation must be rewritten so that less olivine reacts and more spinel is formed. If the composition of pyroxene neoblasts remains the same (actually, it is identical with the composition of PX host) and if there is a constant sum of Cr + Al in the spinel, the younger spinels must be progressively richer in Al and poorer in Cr. This is a clear consequence of the gradually shifting intersection point of tielines OL-PX_{porph} and SPN_{lam}-PX_{neobl} (Fig. 5, inset). Finally, the last spinel to form is the one that exsolved from porphyroclasts in whose breakdown to PX host and SPN lamellae no olivine participates. Inasmuch as the reconstructed original composition of pyroxene porphyroclasts is

Table 5. Chemical composition of spinel

	Cores of large grains		Lamellae in CPX		Lamellae in OPX		Medium and small grains		Grains enclosed in olivine	
	Typical analysis[a]	Range	Typical analysis[a]	Range	Typical analysis[a]	Range	Typical analysis[a]	Range	Typical analysis[a]	Range
SiO_2	0.0(0)	0.0	0.0(0)	0.0	0.0(0)	0.0	0.0(0)	0.0	0.0(0)	0.0
TiO_2	0.06(3)	0.00–0.10	0.03(3)	0.00–0.09	0.0(0)	0.00–0.05	0.0(0)	0.00–0.06	0.0(0)	0.0
Al_2O_3	49.5(2)	49.1–51.5	54.4(2)	53.1–55.7	54.0(2)	53.4–55.2	53.2(2)	52.0–55.7	54.3(2)	50.4–54.7
Cr_2O_3	19.38(9)	18.4–20.0	14.48(8)	13.7–16.4	14.94(8)	13.8–15.3	15.57(8)	14.0–18.4	14.71(8)	14.1–18.8
Fe_2O_3[b]	1.33	0.08–1.87	0.57	0.00–1.60	1.09	0.00–1.20	0.91	0.00–1.07	0.54	0.00–1.50
FeO	10.10(6)	9.8–10.8	9.68(6)	9.4–10.4	9.59(6)	9.5–10.7	9.91(6)	9.9–10.8	10.72(6)	10.3–11.2
MnO	0.13(2)	0.08–0.19	0.10(2)	0.06–0.16	0.10(2)	0.07–0.16	0.15(2)	0.09–0.17	0.10(2)	0.09–0.20
MgO	19.2(1)	18.9–19.6	19.9(1)	19.5–20.4	20.0(1)	19.2–20.2	19.6(1)	18.6–20.0	19.3(1)	18.8–19.7
NiO	0.341(6)	0.33–0.36	0.35[c]		0.35[c]		0.348(6)	0.34–0.37	0.35[c]	
Σ	100.1(2)		99.4(2)		100.1(2)		99.7(2)		100.0(2)	
$\frac{Mg}{Mg + Fe_{tot}}$	0.752(1)	0.748–0.763	0.776(1)	0.762–0.785	0.771(1)	0.754–0.777	0.765(1)	0.750–0.780	0.754(1)	0.732–0.759
Cr/(Cr + Al)	0.208(1)	0.193–0.214	0.1516(9)	0.142–0.172	0.1565(9)	0.144–0.161	0.1640(9)	0.144–0.191	0.1536(9)	0.148–0.200
$\frac{Fe^{3+}}{Fe^{3+} + Cr + Al}$	0.0134	0.0008–0.0212	0.0056	0.0000–0.0186	0.0108	0.0000–0.0172	0.0090	0.0000–0.0130	0.0053	0.0000–0.0162

[a] Errors given are those of individual determinations and were computed according to KOTRBA (1989).
[b] Fe_2O_3 was calculated; accordingly, ratios involving Fe^{3+} do not have errors.
[c] A mean of several determinations most of which come from other analytical points.

known with large errors, there are only mild constraints on the composition of spinel that participated in the reaction, but the above scheme seems to explain the observations.

An interesting insight into the crystallization history of the rock in the xenolith comes from an analysis of spinel exsolution in CPX porphyroclasts. First, the bulk composition recalculated to six oxygens assuming full cation occupancy yields an acceptable pyroxene formula only if all iron is trivalent (Fig. 12, origin of arrow A). Second, spinel in lamellae is very low in (calculated) Fe^{3+} (Table 5, Fig. 7), and the OA phase, when recalculated as orthopyroxene, appears to contain divalent iron only. Third, as can be seen in Fig. 12, if we try to reconstruct the composition of clinopyroxene after unmixing of OPX (OA) lamellae but before unmixing of spinel, we arrive at a point (origin of arrow B) located on a tieline CPX host-SPN lamellae, which lies off the tieline DI-COR. In other words, such a point does not represent a stoichiometric pyroxene formula because it has more than two cations per three oxygens. Thus what has been said indicates that the conditions must have been more oxidizing during crystallization of the porphyroclast (and during the partial melting event?) than during unmixing of lamellae. A reduction during the process would explain all observations, and it may even be argued that the exsolution of spinel is a redox reaction. But what was the reductant?

Let us recall that the composition of clinopyroxene assigns the olivine websterite in our xenolith to mantle xenoliths type A (FREY and PRINZ, 1978). Admittedly, the prevalence of CPX and OPX is not typical of depleted type A mantle xenoliths, but such rocks have been reported (*e.g.*, FUJII and SCARFE, 1982). ARCULUS *et al.* (1984) generalized that oxygen fugacity in type A xenoliths is very low, near

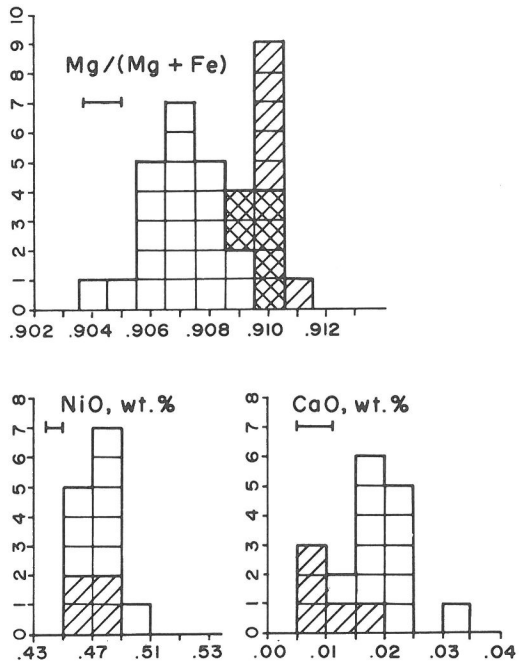

FIG. 11. Distribution of compositional characteristics of olivine; one square represents one determination, the error bar is 2σ in length. Open squares = deformed grains (*i.e.*, cores of grains or outer zones adjacent to pyroxene or another olivine grain); hatched squares = non-deformed grains, 'neoblasts'; cross-hatched squares = outer zones along contact with grains of spinel.

that of the iron-wüstite buffer, while $f(O_2)$ in type B should correspond to the quartz-fayalite-magnetite buffer. Diffusion of hydrogen from a volatile-rich magmatic diapir is thought to be responsible for the low oxygen fugacity in type A xenoliths.

If hydrogen indeed was the all-penetrating reducing agent, we can write an equation for the pro-

Table 6. Chemical composition of olivine

	Deformed grains, cores		Deformed grains, outer zones in contact with SPN		Neoblasts	
	Typical analysis[a]	Range	Typical analysis[a]	Range	Typical analysis[a]	Range
SiO_2	40.8(3)	40.3–41.3	40.9(3)	40.4–41.2	40.7(3)	40.6–41.1
FeO	9.11(6)	8.90–9.20	8.86(6)	8.78–9.05	8.79(6)	8.78–8.89
MnO	0.12(2)	0.06–0.16	0.12(2)	0.06–0.18	0.13(2)	0.12–0.19
MgO	50.0(2)	49.4–50.3	49.9(2)	49.5–50.4	50.0(2)	50.0–50.5
CaO	0.020(3)	0.015–0.032	0.019(3)	0.014–0.020	0.011(3)	0.008–0.015
NiO	0.475	0.458–0.500	0.470(6)	0.467–0.490	0.472(6)	0.455–0.482
Σ	100.5(4)		100.3(4)		100.1(4)	
Mg/(Mg + Fe)	0.9074(6)	0.904–0.909	0.9093(6)	0.909–0.910	0.9102(6)	0.910–0.911

[a] Errors given are those of individual determinations and were computed according to KOTRBA (1989).

Table 7. Calculated temperatures and pressures of equilibration

Phase assemblage	OPX bulk & CPX bulk	OPX host & CPX lamellae	CPX host & OA lamellae	OPX host & CPX host	OPX neoblast
T, °C	1260(100)[a]	880(140)[a]	940(150)[a]	920(140)[a]	900(70)[b]
p, GPa	2.7(7)[c]	1.3(6)[c]	1.7(3)[c]	1.4(6)[c]	1.1(3)[b]

[a] Mean of temperatures according to WELLS (1977), BERTRAND and MERCIER (1986), and MERCIER (1980). As input served mean compositions and their errors. The error for the Bertrand and Mercier thermometer reflects also the error of pressure estimate. The errors given here reflect both the error of the mean and the mean errors for individual algorithms.

[b] Calculated according to MERCIER (1980).

[c] Mean of pressures calculated according to MERCIER (1980) for CPX and OPX.

cess, starting with CPX 'bulk' (obtained from bulk CPX by subtracting appropriate quantity of OA as OPX) and using real compositions of the other phases,

100 CPX 'bulk' + 2.5 H_2 →

96.4 CPX host + 4.8 SPN lam + 2.5 H_2O.

The feasibility of this reaction may be limited by the amount of iron available in the system, but in the present case, this is not a problem. If all iron is reduced to divalent, the projection point of such a composition shifts to the endpoint of the arrow in Fig. 12, beyond the intersection with the CPX host-SPN lamellae tieline, so the above reaction can proceed without restriction. Corresponding to 100 CPX 'bulk' is 7.02 OPX lamellae (now OA), which means that the reaction produces 2.5 OH per seven R^{2+} in OPX lamellae. The ideal stoichiometry of anthophyllite is 2.0 OH per seven Mg. If, moreover, the Fe in OPX lamellae too was reduced from Fe^{3+}, which appears inevitable, the process would free an additional 0.4 OH, making a total of about 2.9 OH available per seven R^{2+}. The lingering uncertainties concerning the identity of the orthoamphibole-like phase notwithstanding, the process offers a convenient sink for some of the hydrogen migrating through the rock. The synthesis of water at the location where it is used to form a hydrated phase makes the case appealing. If the water needed for the conversion of the thin OPX lamellae to OA in the present xenolith or to a sheet silicate at Deštná (ŠANC and RIEDER, 1983) were supplied to the large porphyroclasts from outside, one would expect the process to freeze at some distance from grain boundaries, at least in some grains, and one would not obtain a product in the form of single crystals perfectly crystallographically aligned, but rather a polycrystalline aggregate.

We do not see an analogous process in OPX porphyroclasts, and the reasons are easy to understand. Clinopyroxene in lamellae (like elsewhere) is resistant to hydration and remains intact, and the quantity of water formed by a reaction analogous to the one above is apparently insufficient to cause changes in the OPX host which are detectable by X-ray diffraction.

Interestingly, the same chemical trends that were observed in spinel can be observed in spinel enclosed in olivine, which means that volatiles must have had access to that spinel, perhaps during an event like recrystallization of olivine. It should be mentioned that deformed olivine grains contain veils of bubbles (Fig. 3), apparently filled with volatiles, but not so olivine neoblasts. If the volatiles were produced in situ by a drop in pressure, then the neoblasts either contained no volatiles or formed at lower pressures (see KIRBY and GREEN, 1980).

The exsolution in porphyroclasts and the recrystallization process took place at temperatures we attempted to calculate using three geothermometers (Table 7) applied to pairs, OPX host & CPX lamellae, CPX host & OA lamellae (recalculated as OPX), OPX host & CPX host, and OPX neoblast alone. The resulting temperatures are quite close to one another, with a mean 910°C. It is interesting that the temperature involving the OA phase (recalculated as OPX) fits well into the range obtained. Thus the alteration of the original orthopyroxene must have proceeded with little or no cation exchange. The same was true of the layer silicate in CPX from Deštná (ŠANC and RIEDER, 1983).

As an independent check of these temperatures, we considered the pair olivine & spinel. A number of thermometers have been put forth (EVANS and FROST, 1975; FUJII, 1978; FABRIÈS, 1979; ROEDER *et al.*, 1979) and reviewed (OZAWA, 1983), but the results must be interpreted carefully because of the relatively easy re-equilibration along contacts of OL and SPN grains. In order to arrive at meaningful compositions, we had to have an idea about the chemical variations in both phases. The cores of

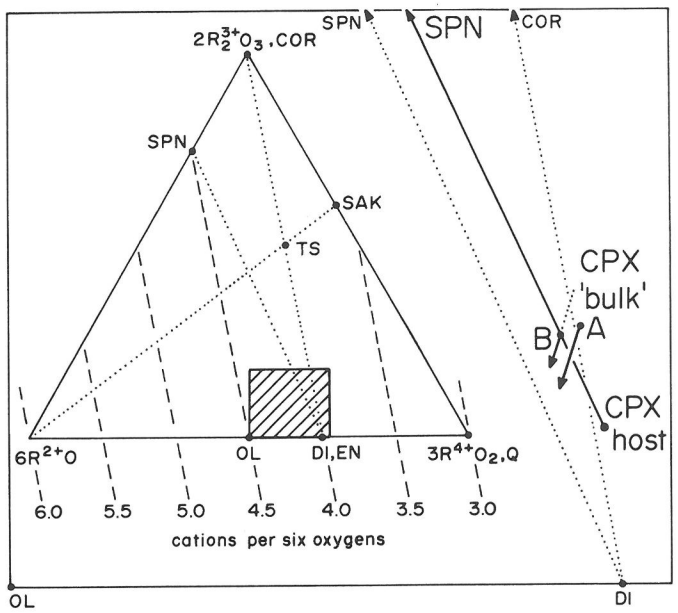

FIG. 12. This figure is an enlargement of the hatched rectangle in the inset and shows that during the unmixing of spinel from clinopyroxene, oxygen is removed from the system (see dashed isolines). DI = diopside; EN = enstatite; Q = quartz; SAK = Al_2SiO_5 phases; COR = corundum; TS = Tschermak's molecules. The CPX host and SPN lamellae are joined with the full line, and point B represents the composition of their intergrowth. Point A was obtained by subtracting orthoamphibole lamellae (as OPX) from the analytical bulk composition of CPX porphyroclasts. The endpoints of arrows represent compositions with all iron recalculated as divalent. The two arrows would coincide if not for errors associated (mainly) with planimetering the decomposed porphyroclasts. Points A and CPX host fall off the DI-COR line because no correction was made for the univalent cations present in small quantities.

deformed olivine grains (about 90 vol.% of all olivine) appear homogeneous, but in the border zone, there is an increase of forsterite component towards contacts with spinel (Fig. 13). The composition of these zones is like that of small undeformed olivine grains, and both apparently formed at the same time; neither was usable for our purposes. Spinel grains exhibit a small but systematic decrease of the

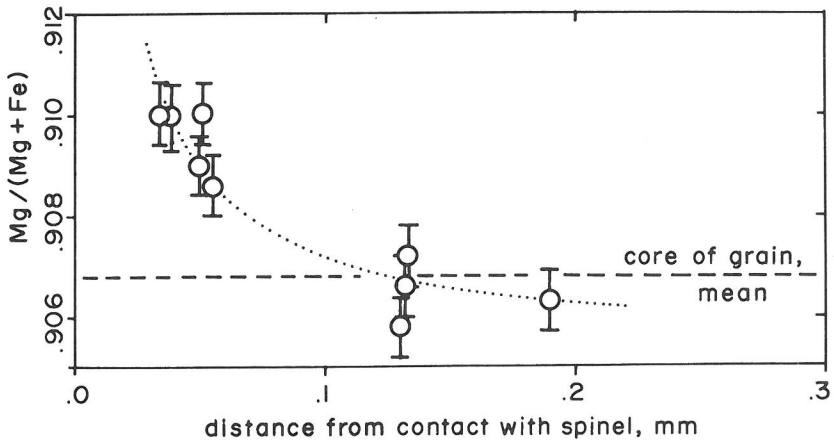

FIG. 13. The composition of outer zones of olivine grains changes towards their contacts with grains of spinel. The error bar represents $\pm 1\sigma$.

$Mg/(Mg + Fe_{tot})$ ratio towards neighboring olivine grains and they always show a lower $Mg/(Mg + Fe_{tot})$ than spinel grains of the same size surrounded by pyroxenes only (Fig. 10). These too had to be avoided. In the end, we used the algorithm of FABRIÈS (1979) and applied it to the composition of cores of deformed olivine grains and the composition of large spinel grains surrounded by pyroxene. The resulting temperatures have a smaller scatter about 830(±25)°C, and the similarity of this temperature to that based on the other thermometers suggest that all these data pertain to the last detectable thermal event in the history of the xenolith.

The chemical changes observed, particularly those along contacts of grains of different minerals, are probably due either to reactions during cooling (OZAWA, 1983) or during a short-term low-temperature event such as metamorphism of the granulite. Indeed, temperatures based on the compositions of border zones of olivine and spinel are lower than for recrystallization, between 680 and 800°C, but our data do not confirm the relation of temperature to the size of spinel grains (OZAWA, 1983).

There is no dependable geobarometer for the association OPX + CPX + OL + SPN, and thus the processes described above are difficult to characterize by reliable estimates of pressure. The absence of plagioclase and the very low contents of Ca in olivine nevertheless indicate that the pressures must have been those typical of the stability field for spinel peridotite. An estimation of pressure from the Ca content of olivine according to ADAMS and BISHOP (1986) might be incorrect since the barometer is based on experimental data for high temperatures. True, there are pressure estimates based on the one-pyroxene barometer of MERCIER (1980), but the results must be viewed with caution, particularly for the reconstructed bulk compositions of the porphyroclasts. Let it be mentioned though that pressures obtained for subsolidus phases in porphyroclasts (Table 7) are close to those reported by PIN and VIELZEUF (1988) for granulites from Zrcadlová huť (L2) and Blanský les (L9). Their pressures are based on the garnet-Al_2SiO_5-quartz geobarometer, and the mean corresponding to 800°C is 1.57 GPa. While the exsolution in pyroxenes in the xenolith may or may not have taken place at the time of crystallization of the enclosing granulite, it is likely that both events proceeded at similar depths.

Acknowledgements—Stimulating discussions on some aspects of analytical work were held with Ing. Z. Kotrba and Ing. R. Rybka. The manuscript was critically read by Dr. S. Vrána and Dr. K. Vokurka (all Geological Survey, Prague). The reviews by Dr. M. E. Fleet and Dr. G. L. Nord helped clarify presentation and resulted in a general improvement. This paper is an extention of the senior author's RNDr. Thesis defended at Charles University in 1985.

REFERENCES

ADAMS G. E. and BISHOP F. C. (1986) The olivine-clinopyroxene geobarometer: experimental results in the CaO-FeO-MgO-SiO_2 system. *Contrib. Mineral. Petrol.* **94,** 230–237.

AFTALION M., BOWES D. R. and VRÁNA S. (1989) Early Carboniferous U-Pb zircon age for garnetiferous, perpotassic granulites, Blanský les massif, Czechoslovakia. *N. Jb. Miner. Mh.* **1989,** 145–152.

ANDERSEN T., O'REILLY S. Y. and GRIFFIN W. L. (1984) The trapped fluid phase in upper mantle xenoliths from Victoria, Australia: implications for mantle metasomatism. *Contrib. Mineral. Petrol.* **88,** 72–85.

ARCULUS R. J., DAWSON J. B., MITCHELL R. H., GUST D. A. and HOLMES R. D. (1984) Oxidation states of the upper mantle recorded by megacryst ilmenite in kimberlite and type A and B spinel lherzolite. *Contrib. Mineral. Petrol.* **85,** 85–94.

BASU A. R. and MACGREGOR I. D. (1975) Chromite spinels from ultramafic xenoliths. *Geochim. Cosmochim. Acta* **39,** 937–945.

BENCE A. E. and ALBEE A. L. (1968) Empirical correction factors for the electron microanalysis of silicates and oxides. *J. Geol.* **76,** 382–403.

BERGMAN S. C. and DUBESSY J. (1984) CO_2-CO fluid inclusions in a composite peridotite xenolith: implications for upper mantle oxygen fugacity. *Contrib. Mineral. Petrol.* **85,** 1–13.

BERTRAND P. and MERCIER J.-C. C. (1986) The mutual solubility of coexisting ortho- and clinopyroxenes: toward an absolute geothermometer for the natural systems? *Earth Planet. Sci. Lett.* **76,** 109–122.

BURNHAM C. W. (1962) Lattice constant refinement. *Carnegie Inst. Wash. Yearb.* **61,** 132–135.

DICK H. J. B. (1977a) Evidence for partial melting in the Josephine Peridotite. *Oregon Dept. Geol. Min. Ind. Bull.* **96,** 59–63.

DICK H. J. B. (1977b) Partial melting in the Josephine Peridotite I, the effect on mineral composition and its consequence for geobarometry and geothermometry. *Amer. J. Sci.* **277,** 801–832.

DICK H. J. B. and BULLEN T. (1984) Chromian spinel as a petrogenetic indicator in abyssal and alpine-type peridotites and spatially associated lavas. *Contrib. Mineral. Petrol.* **86,** 54–76.

DICKEY J. S., JR. and YODER H. S., JR. (1972) Partitioning of chromium and aluminum between clinopyroxene and spinel. *Carnegie Inst. Wash. Yearb.* **71,** 384–392.

DICKEY J. S., JR., YODER H. S., JR. and SCHAIRER J. F. (1971) Chromium in silicate-oxide systems. *Carnegie Inst. Wash. Yearb.* **70,** 118–122.

EALES H. V. and MARSH J. S. (1983) Al/Cr ratios of coexisting pyroxenes and spinellids in some ultramafic rocks. *Chem. Geol.* **38,** 57–94.

EVANS B. W. and FROST B. R. (1975) Chrome-spinel in progressive metamorphism—a preliminary analysis. *Geochim. Cosmochim. Acta* **39,** 959–972.

FABRIÈS J. (1979) Spinel-olivine geothermometry in peridotites from ultramafic complexes. *Contrib. Mineral. Petrol.* **69,** 329–336.

FEDIUKOVÁ E. (1965) Ultrabasic xenoliths in the granulite

at Mt. Kleť near Český Krumlov. *Acta Univ. Carol., Geol.* **1965,** 189–202.

FEDIUKOVÁ E. (1978) Mafic minerals from granulites of the borehole Holubov (South Bohemian Moldanubicum). *Sbor. geol. věd, lož. geol., mineral.* **19,** 169–198.

FIALA J., MATĚJOVSKÁ O. and VAŇKOVÁ V. (1987) Moldanubian granulites and related rocks: petrology, geochemistry and radioactivity. *Rozpravy Československ. akad. věd, řada mat. přír. věd* **97,** 1–102.

FLEET M. E. (1981) The intermediate plagioclase structure: an explanation from interface theory. *Phys. Chem. Minerals* **7,** 64–70.

FLEET M. E. (1982) Orientation of phase and domain boundaries in crystalline solids. *Amer. Mineral.* **67,** 926–936.

FREY F. A. and PRINZ M. (1978) Ultramafic inclusions from San Carlos, Arizona: Petrologic and geochemical data bearing on their petrogenesis. *Earth Planet. Sci. Lett.* **38,** 129–176.

FUJII T. (1978) Fe-Mg partitioning between olivine and spinel. *Carnegie Inst. Wash. Yearb.* **76,** 563–569.

FUJII T. and SCARFE C. M. (1982) Petrology of ultramafic nodules from West Kettle River, near Kelowna, southern British Columbia. *Contrib. Mineral. Petrol.* **80,** 297–306.

GREEN D. H. (1964) The petrogenesis of the high-temperature peridotite intrusion in the Lizard area, Cornwall. *J. Petrol.* **5,** 134–188.

GREEN D. H. and RINGWOOD A. E. (1967) The genesis of basaltic magmas. *Contrib. Mineral. Petrol.* **15,** 103–190.

HANIC F., MAĎAR J. and KISS V. (1955) Precession X-ray diffraction camera. *Czechoslovak Patent 89363* (in Slovak).

HENDERSON P. (1975) Reaction trends shown by chrome-spinels of the Rhum layered intrusion. *Geochim. Cosmochim. Acta* **39,** 1035–1044.

IRVINE T. N. (1967) Chromium spinel as a petrogenetic indicator. Part 2. Petrologic applications. *Can. J. Earth Sci.* **4,** 71–103.

JAQUES A. L. and GREEN D. H. (1980) Anhydrous melting of peridotite at 0–15 kb pressure and the genesis of tholeiitic basalts. *Contrib. Mineral. Petrol.* **73,** 287–310.

KIRBY H. S. and GREEN H. W. (1980) Dunite xenoliths from Hualalai volcano: evidence for mantle diapiric flow beneath the Island of Hawaii. *Amer. J. Sci.* **280-A,** 550–575.

KODYM O. (1972) Multiphase deformation in the Blanský les granulite massif (South Bohemia). *Krystalinikum* **9,** 91–105.

KODYM O., JAKEŠ P. and SCHOVÁNEK P. (1978) Granulite und ultramafische Gesteine aus der Strukturbohrung Holubov. *Sbor. geol. věd, Geol.* **32,** 7–41.

KOTRBA Z. (1989) Recent advances in X-ray microanalysis. *Rudy* **37,** 15–19 (in Czech).

KUO L.-C. and ESSENE E. J. (1986) Petrology of spinel harzburgite xenoliths from the Kishb Plateau, Saudi Arabia. *Contrib. Mineral. Petrol.* **93,** 335–346.

MERCIER J.-C. C. (1980) Single-pyroxene thermobarometry. *Tectonophysics* **70,** 1–37.

MERCIER J.-C. C. and NICOLAS A. (1975) Textures and fabrics of upper-mantle peridotites as illustrated by xenoliths from basalts. *J. Petrol.* **16,** 454–487.

MYSEN B. O. and KUSHIRO I. (1977) Compositional variations of coexisting phases with degree of melting of peridotite in the upper mantle. *Amer. Mineral.* **62,** 843–865.

OBATA M. (1980) The Ronda peridotite: garnet-, spinel-, and plagioclase-lherzolite facies and the *P-T* trajectories of a high-temperature mantle intrusion. *J. Petrol.* **21,** 533–572.

OZAWA K. (1983) Evaluation of olivine-spinel geothermometry as an indicator of thermal history for peridotites. *Contrib. Mineral. Petrol.* **82,** 52–65.

OZAWA K. (1988) Ultramafic tectonite of the Miyamori ophiolitic complex in the Kitakami Mountains, Northeast Japan: hydrous upper mantle in an island arc. *Contrib. Mineral. Petrol.* **99,** 159–175.

PIN C. and VIELZEUF D. (1988) Les granulites de haute-pression d'Europe moyenne témoins d'une subduction éo-hercynienne. Implications sur l'origine des groupes leptyno-amphiboliques. *Bull. Soc. géol. France (8)* **IV,** 13–20.

RIEDER M. (1971) A FORTRAN IV computer program for calculating high-precision cubic cell edges by extrapolation. *Věst. Ústřed. ústavu geol.* **46,** 65–76.

ROBINSON P., ROSS M., NORD G. L., JR., SMYTH J. R. and JAFFE H. W. (1977) Exsolution lamellae in augite and pigeonite: fossil indicators of lattice parameters at high temperature and pressure. *Amer. Mineral.* **62,** 857–873.

ROEDER P. L., CAMPBELL I. H. and JAMIESON H. E. (1979) A re-evaluation of the olivine-spinel geothermometer. *Contrib. Mineral. Petrol.* **68,** 325–334.

ROST F. (1966) Über ultrabasische Einschlüsse in metamorphen Gesteinen des südlichen Moldanubikums. *Krystalinikum* **4,** 127–162.

ŠANC I. (1982) Mean thermal expansion coefficients of diopside and enstatite cell parameters and their petrologic significance. *Acta Univ. Carol., Geol.* **1981,** 427–435.

ŠANC I. and RIEDER M. (1983) Lamellar pyroxenes and their petrogenetic significance: three examples from the Czech Massif. *Contrib. Mineral. Petrol.* **84,** 73–83.

SKINNER B. J. (1966) Thermal expansion. In *Handbook of Physical Constants* (ed. S. P. CLARK, JR.), Sec. 6, pp. 75–96. *Geol. Soc. Amer. Mem.* **97.**

SLABÝ J. (1983) Modal composition and petrochemistry of granulites of the Lišov and Blanský les Mts. massifs, southern Bohemia. *Čas. mineral. geol.* **28,** 41–60 (in Czech).

STRECKEISEN A. (1973) Classification and nomenclature of plutonic rocks: recommendations. *N. Jb. Mineral. Mh.* **1973,** 149–164.

VAN BREEMEN O., AFTALION M., BOWES D. R., DUDEK A., MÍSAŘ Z., POVONDRA P. and VRÁNA S. (1982) Geochronological studies of the Bohemian massif, Czechoslovakia, and their significance in the evolution of Central Europe. *Trans. Roy. Soc. Edinburgh, Earth Sci.* **73,** 89–108.

VRÁNA S. (1979) Polyphase shear folding and thrusting in the Moldanubicum of southern Bohemia. *Věst. Ústřed. ústavu geol.* **54,** 75–86.

VRÁNA S. (1987) Garnet-fassaitic pyroxene skarn from the granulite complex of southern Bohemia. *Věst. Ústřed. ústavu geol.* **62,** 193–206.

WELLS P. R. A. (1977) Pyroxene thermometry in simple and complex systems. *Contrib. Mineral. Petrol.* **62,** 129–139.